JOURNAL OF MATERIALS SCIENCE 23 (1988) 2429–2443

The erosion behaviour of TiN coatings on steels

P. J. BURNETT*, D. S. RICKERBY
Materials Development Division, Harwell Laboratory, Didcot, Oxfordshire OX11 0RA, UK

The erosion behaviour of physical vapour-deposited titanium nitride has been studied using both blunt particle and angular particle erodent streams. The mechanisms of erosive loss have been identified and related to the microstructure and internal stress state of the coatings. High levels of internally stored energy (which scales with coating thickness and internal stress) induce spalling in erosion testing using blunt erodents. Consequently, it is found that thick coatings are more resistant to angular particle erosion whilst thin coatings have longer lifetimes when exposed to blunt erodents. Scratch adhesion testing has been performed on all erosion specimens and attempts made to correlate the critical load for coating failure, with the failure mechanisms observed in erosive wear. Whilst no correlation can be found between erosion resistance and critical load, good correlations between the failure mechanisms found in erosion and scratch testing can be made.

1. Introduction

The use of ceramic coatings in industry is increasing, thermal barrier coatings (prepared by plasma-spraying techniques, e.g. [1]) and wear resistant coatings (e.g. [2–4]) being two of the most important areas of interest. The latter class of coatings includes materials such as titanium nitride and titanium carbide produced by either chemical vapour deposition (CVD) or physical vapour deposition (PVD) techniques. The present paper will focus on the erosion behaviour of PVD coatings because, as PVD coating technology becomes both more reliable and more readily available, potential applications in erosive environments such as petrochemical plant and gas turbines are being investigated. Clearly, whilst it is desirable to be able to "predict" the response of a given coating in an erosive environment without recourse to expensive field trials, little information concerning the erosion behaviour of wear-resistant coatings is to be found in the literature. Levy *et al.* [5] have studied the erosion behaviour of CVD silicon carbide wear-resistant coatings and concluded (i) the finer the coating grain size the greater the erosion resistance, and (ii) that in order to prevent catastrophic failure the coating had to be greater than 100 μm thick. However, most commercially available PVD coatings are usually less than 20 μm thick for which there are few data concerning their erosion behaviour. Jonsson *et al.* [6] have studied the erosion behaviour of 1 μm reactive magnetron sputtered TiN subjected to erosion by angular quartz particles and attempted to correlate the time-to-coating loss with the practical levels of adhesion as revealed by single-pass scratch tests. These workers found little difference between the scratch behaviour of their test samples, but did find significant differences between their erosion resistance. They concluded that erosion testing might be a more sensitive means of assessing levels of "practical adhesion" than scratch testing. The "practical adhesion level" corresponds to the amount of additional mechanical energy that is required to detach a coating from a given substrate and it is important to differentiate between this and the theoretical and/or interfacial adhesion. The former reflects the net effect of all of the forces acting on the interface and includes both the effects of residual internal stress within the coating [7, 8] and the mechanical stresses imposed by the loading geometry. The latter reflects only the bonding forces across the coating/substrate interface. For instance, the practical adhesion of oxides subjected to erosion, i.e. the critical particle velocity above which the oxide spalls, is not only governed by the oxide/substrate bond strength, but also by the coating thickness, coating strength and substrate properties [9, 10]. Similarly, in the scratch adhesion test (rapidly becoming the industry standard for adhesion testing [11–13]) a diamond stylus is drawn across a coated surface at ever increasing loads until at a critical load, L_c, the coating is stripped from the track; L_c is found to depend strongly on thickness, coating properties and substrate properties. In addition to these measures of "practical adhesion", shock wave loading [14, 15] and static indentation adhesion testing [16–18] have been used and are analogous to erosion and scratch testing, respectively [13, 19]. Given that both erosion behaviour and scratch testing reflect practical adhesion levels, albeit made under differing mechanical stimuli, it would be useful to be able to correlate results obtained from scratch testing to erosion behaviour.

The aim of the present paper is to describe the erosion behaviour of thick and thin PVD titanium nitride coatings when subjected to sharp and blunt erodent particles. In addition, the use of two substrate materials has allowed the production of high and low internal stress levels (this being thought to strongly

---

* *Present address*: Shell Research Ltd, Thornton Research Centre, P.O. Box 1, Chester CH1 3SH, UK.

0022–2461/88 $03.00 + .12 © *1988 Chapman and Hall Ltd.*

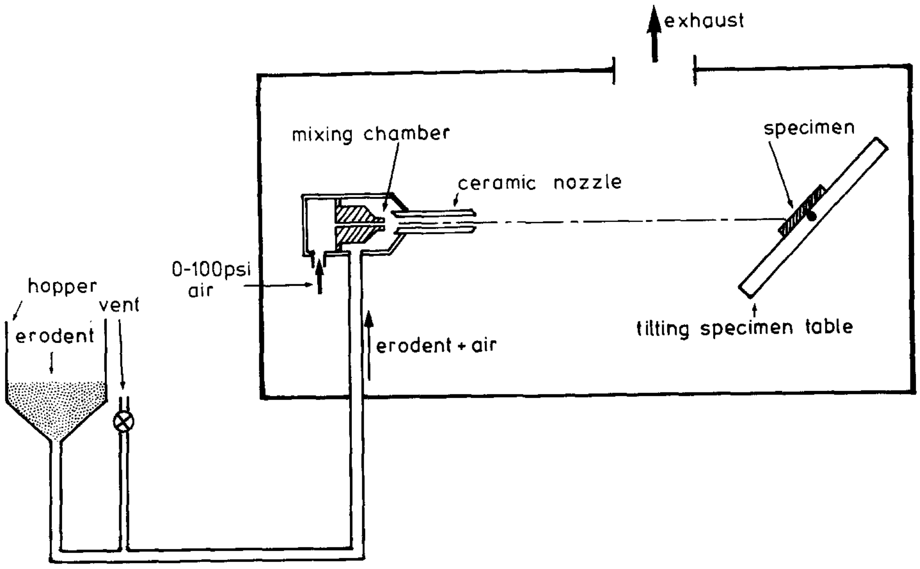

Figure 1 A schematic diagram of the erosion apparatus (not to scale).

influence practical adhesion). Hardness and scratch adhesion testing have been carried out on all erosion specimens and attempts will be made to correlate these data with the erosion behaviour.

2. Experimental procedure

2.1. Specimen preparation

Coupons of stainless steel (18% Cr, 9% Ni, 1% Ti all in wt %) and "20"-carbon steel (formerly grade En3B; 0.25% C, 0.35% Si, 1.00% Mn all in wt %) were cut to size (~25 mm × 70 mm × 4 mm), ground on successively finer silicon carbide papers and polished to mirror finish using a 3 μm diamond paste impregnated wheel. After degreasing, these specimens were coated with titanium nitride using the sputter-ion-plating (SIP) facility at Harwell Laboratory (this technique is described in detail elsewhere [20, 21]). Prior to coating with TiN, the coupons were further pre-cleaned by ion bombardment at −500 V followed by the deposition of a thin ($\lesssim$ 100 nm) titanium interlayer in order to improve coating adhesion [22, 23]. The titanium nitride coatings were deposited at a temperature of ~500° C with a deposition rate of 0.2 to 0.5 μm h^{-1}. The coupons were biased 50 V negative with respect to earth to induce ion bombardment of the coatings during deposition and thereby promote the formation of a dense, fine-grained coating [24–26].

The thickness of the coatings was determined on metallographic cross-sections and spanned the range 1 to ~10 μm (see Table I).

2.2. Erosion testing

Erosion testing was carried out using a modified Guyson bead blasting cabinet fitted with a vacuum feed hopper (Fig. 1). The hopper was repeatedly charged with a known mass of erodent (usually ~14 g) and the specimens examined with light microscopy between each charge. The specimens were held in a jig ~140 mm from the nozzle (~6 mm internal diameter × ~80 mm long) and were angled at either 45° or 90° to the erodent stream. A tantalum mask with a 1 cm diameter hole was placed over the specimens allowing only the central portion of the erodent stream (~30 mm diameter) to come into contact with the coated surface. This allowed more than one erosion test to be carried out on a given coupon and also permitted scratch adhesion and hardness testing to be carried out adjacent to the eroded areas. Both blunt erodent particles (80 to 120 mesh glass beads; Fig. 2a) and angular grits (60 to 80 mesh alumina; Fig. 2b) were used with particle velocities between 14 and 35 m sec^{-1} (determined using the double disc method [27]) and a mass flow rate of ~1 g sec^{-1}. As loss of coating was rapid and, being interested

TABLE I Coating thickness, hardness, internal stress and scratch adhesion values for TiN on steels

Substrate	Thickness (μm)	Hardness parameters (see Equation 1)			Scratch adhesion results		Internal stress (MPa)
		$H_{10\mu m}$	a	m	Critical load (g)	Principal failure mode	
"20"-carbon steel	1.5	–	–	–	1900 ± 200	Buckling and tensile cracking and conformal cracking	–
	3.6	2500	4988	1.7	3100 ± 200	Conformal cracking and coating loss	−3960 ± 110
	7.0	–	–	–	3500 ± 200	Regular chipping	–
	10.5	2750	4358	1.8	6300 ± 200	Cohesive chipping	−3680 ± 230
18/9/1 stainless steel	1.4	–	–	–	1300 ± 200	Conformal cracking and loss of coating from track	–
	3.0	2650	5049	1.72	1700 ± 100	Buckling, chipping and spalling	−6320 ± 30
	7.0	–	–	–	3100 ± 300	Chipping and spalling	–
	10.0	3000	5334	1.75	3000 ± 500	Spalling	−5730 ± 250

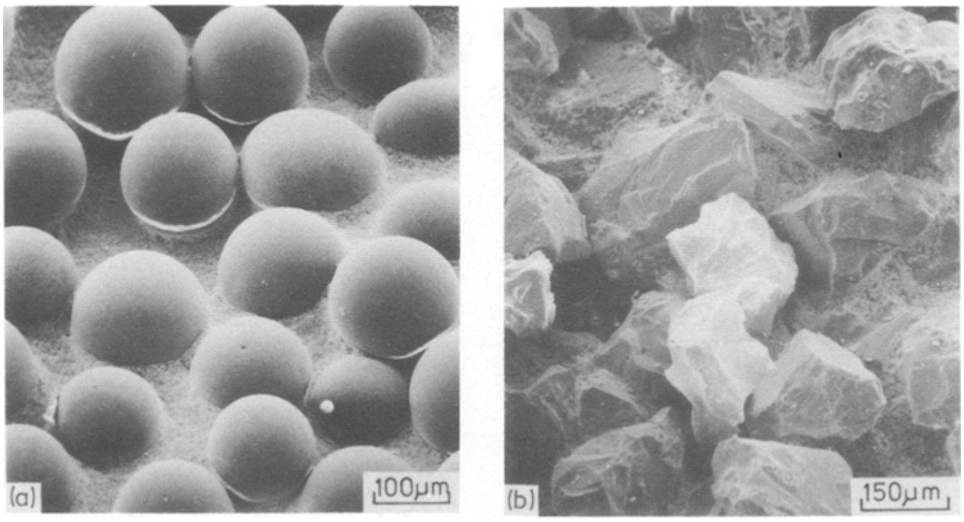

Figure 2 Scanning electron micrographs of the erodent particles used in this study. (a) Glass beads, (b) alumina grit.

principally in relative erosion resistance in this study, only the mass of erodent required to cause total coating loss was determined in each case. Some tests were stopped prematurely to allow scanning electron microscopy (SEM) studies of the developing erosion scars to be made.

2.3. Hardness testing

Hardness testing was performed on all erosion specimens in areas close to the erosion scars. A Shimadzu microhardness tester was used over a load range of 15 to 1000 gf (~147 to 9807 × 10^{-3} N). A Vickers profile indentor was employed with indentor dwell times of 15 sec. The resultant hardness–load data for the coating/substrate composite were analysed using the model described by Burnett and Rickerby [28, 29]. This allows the "true" hardness behaviour of the coating to be extracted from the composite experimental hardness* and incorporates the intrinsic variation of hardness with indentation size (the indentation size effect, ISE) observed for many materials (e.g. [30]). Thus, the hardness behaviour of the coating may be expressed as follows

$$H(d) = ad^{m-2} \quad (1)$$

where $H(d)$ is the coating hardness at diagonal d, a is a constant and m is the indentation size effect index.

2.4. Scratch adhesion testing

Scratch adhesion testing was performed using commercially available equipment (Centre Suisse D'Electronique et de Microtechnique, Neuchatel, Switzerland) fitted with a Rockwell "C" diamond stylus (cone apex angle 120°, tip radius 200 μm). In this test the critical load, L_c, for loss of coating adhesion is determined by increasing the normal load used for scratching until regular coating failure occurs along the whole length of the scratch track. Coatings may fail in a number of ways including regular chipping from the edges, spallation or loss of coating from the bottom of the track (see [11–13, 31]). The load range used was 100 gf to 10 kgf (~980 × 10^{-3} to 98 N) and the critical load determined by examination of the scratch tracks using light microscopy.

2.5. X-ray stress measurements

The level of internal or residual stress present in a PVD coating consists of two components; (i) a thermal expansion mismatch stress generated when the coating and substrate are cooled from the deposition temperature, and (ii) an intrinsic or growth stress resulting from interaction between the growing crystallites which make up the coating [7]. Generally, the internal stresses generated for TiN deposited on to steels are compressive and values in excess of 5 GPa have been reported by the present authors [7, 24, 25].

The internal stresses present in the SIP-TiN coatings studied here were measured using the $\sin^2 \psi$ method (described in detail elsewhere [7, 8]) using Cu$K\alpha$ radiation on an APEX diffractometer. The high-angle (4 2 2) diffraction peaks were used where possible to ensure a high precision.

3. Results

3.1. Microstructure and internal stress

The coatings produced by the sputter-ion-plating process exhibit the columnar microstructure typical of many PVD processes and Fig. 3 shows both cross-sectional and plan views of a SIP coating. The internal stress levels determined using the $\sin^2 \psi$ X-ray technique are given in Table I, where it can be seen that the stresses are greater for the TiN on stainless steel than for TiN on "20"-carbon steel. This can be attributed principally to the greater thermal expansion coefficient mismatch for the stainless steel substrate. It is also apparent that the thicker (10 μm) coatings show lower levels of internal stress than the thinner (3 μm) coatings. This is a consequence of "stress averaging" over the thickness of the coating sampled by the X-ray technique. The lower stress measured in the thicker

---

*For thin PVD films it is impossible to obtain hardness data that arise solely from the coating because in the load ranges conventionally used some deformation of the substrate inevitably occurs [28, 29].

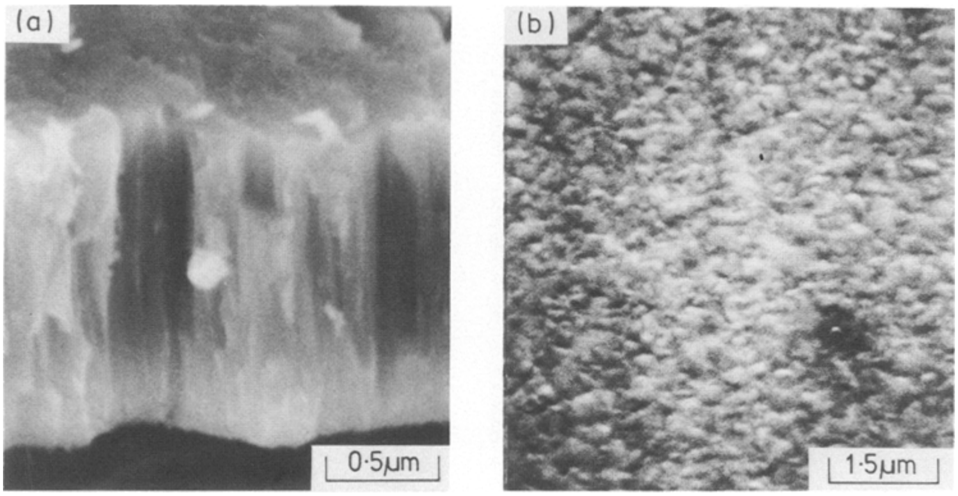

Figure 3 Scanning electron micrographs showing the typical columnar growth morphology of PVD–TiN coatings. (a) Cross-section, (b) plan view.

coating is thought to reflect increasing porosity in the film as it grows to greater thicknesses [24, 25].

3.2. Erosion

The mass of erodent for coating loss (as determined using optical microscopy) for erosion of 3 and 10 μm TiN coatings on stainless and "20"-carbon steel substrates are shown in Figs 4 and 5, respectively. Erosion tests using both glass beads at 35 and 24 m sec^{-1} at 45° angle of incidence and alumina grits at 14 m sec^{-1} at 90° incidence were carried out. It is clear from Figs 4 and 5 that for both erosion conditions the TiN coatings on "20"-carbon steel were the more erosion resistant. However, it can also be seen that whilst the thicker coatings provided enhanced erosion resistance when subjected to erosion by the alumina grits (Fig. 4), the thinner coatings appeared to be more erosion resistant when impacted by glass beads (Fig. 5).

Scanning electron microscopy (SEM) indicates that during bombardment by angular particles the erosion mechanism for TiN coatings on both stainless steel and carbon steel substrates is predominantly by chipping (Fig. 6); with thinner coatings gross "ploughing" deformation is observed, both the coating being pushed ahead of grooves and pits formed by the impacting erodent particles (e.g. Fig. 7a). Alternatively, for the TiN/stainless steel coupons spallation of the coating may also occur and Fig. 7b shows an area of coating that has been pushed ahead of an impacting particle around which the coating has spalled. On the thicker coatings the deformation is much more limited

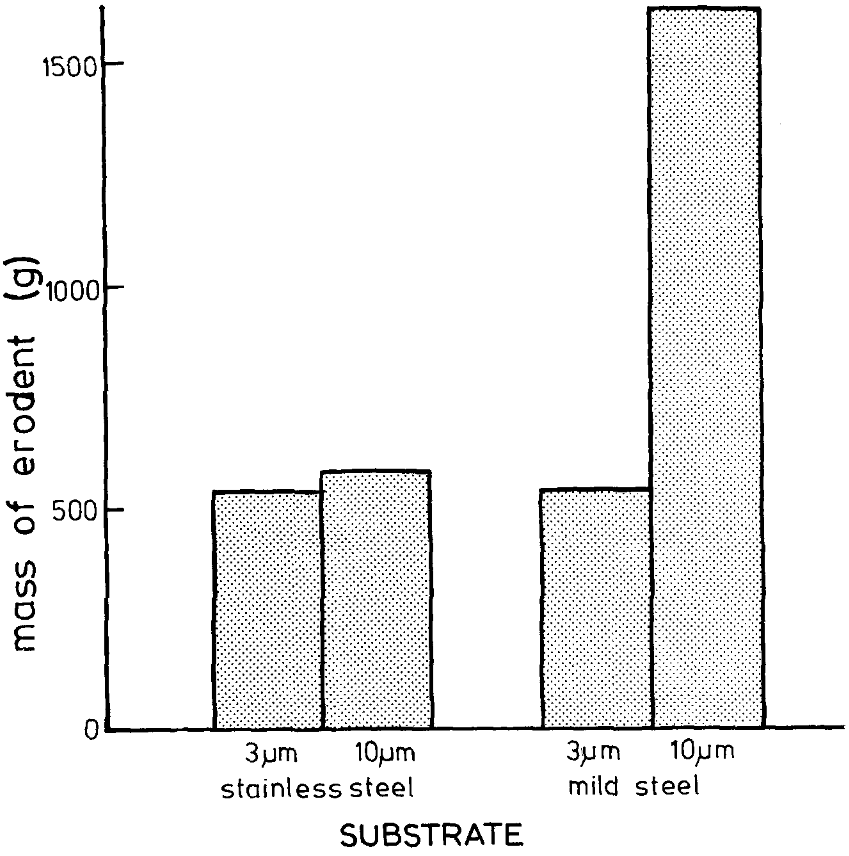

Figure 4 The mass of erodent for coating loss by angular erosion (angle of incidence = 90°) for stainless steel and "20"-carbon steel (mild steel) substrates coated with SIP-TiN to two thicknesses. Erodent, alumina grit. Velocity 14 m sec^{-1}.

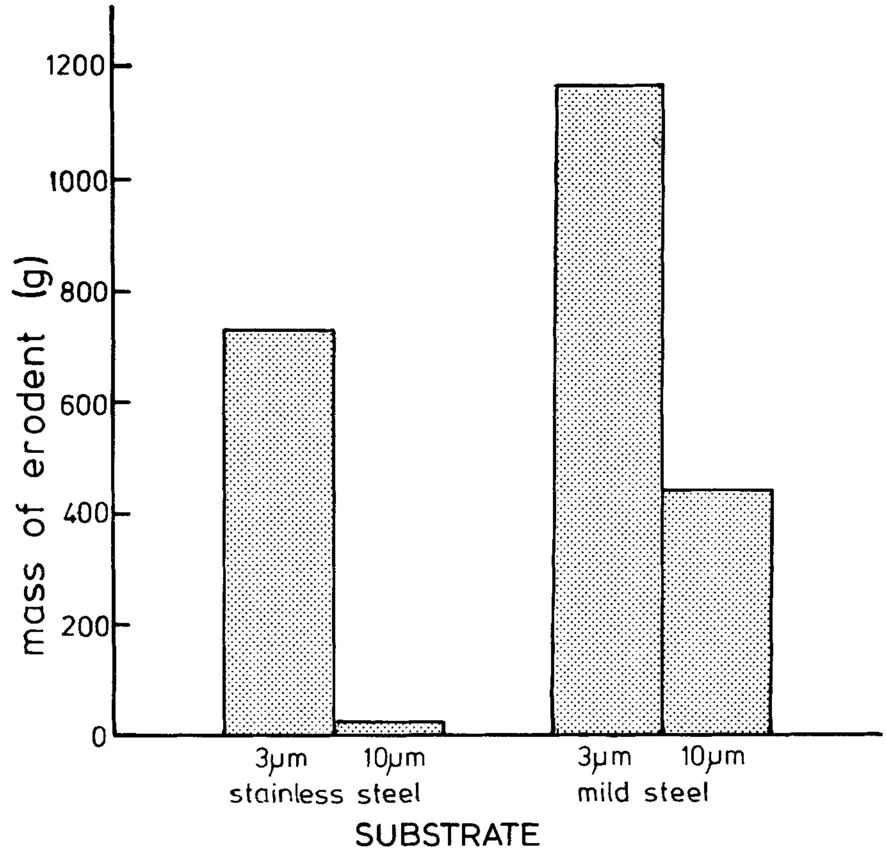

Figure 5 The mass of erodent for coating loss by blunt erosion (angle of incidence = 45°) for stainless steel and "20"-carbon steel (mild steel) substrates as coated with SIP–TiN to two thicknesses. Erodent, glass beads. Velocity 24 m sec^{-1}.

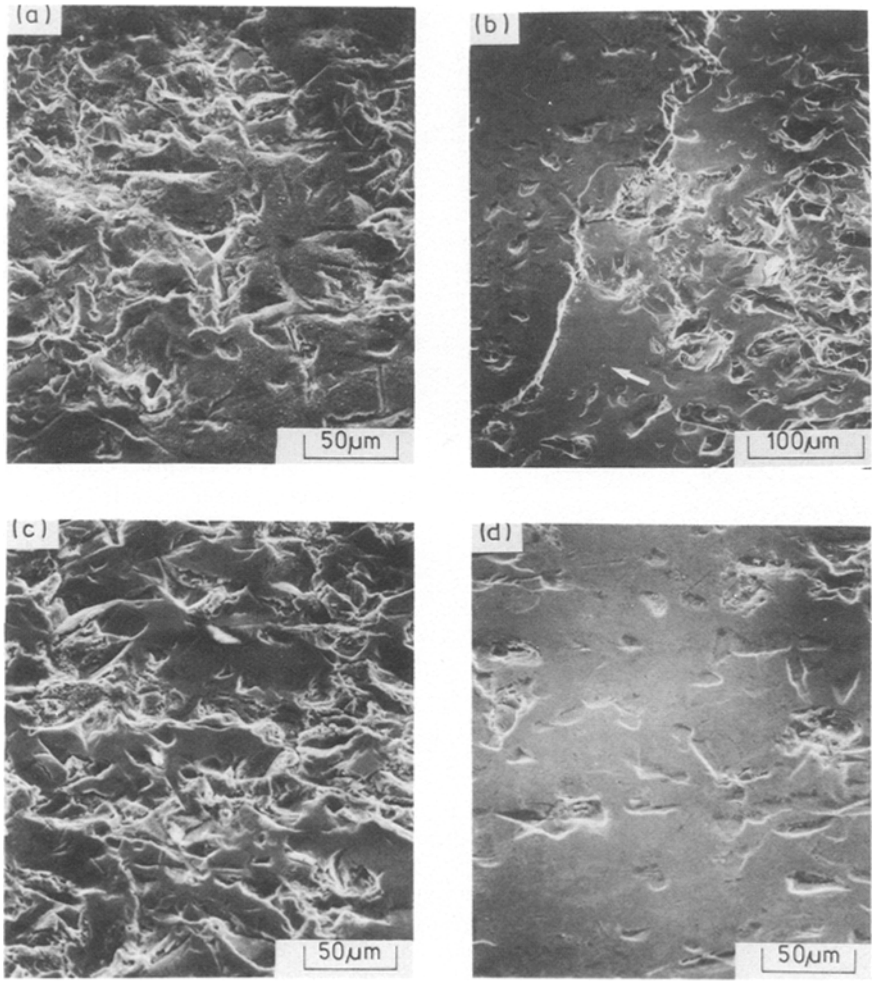

Figure 6 Scanning electron micrographs of TiN-coated steels lightly eroded using alumina grits at 14 m sec^{-1}. (a) 3 μm TiN on stainless steel, (b) 10 μm TiN on stainless steel, (c) 3.6 μm TiN on "20"-carbon steel and (d) 10.5 μm TiN on "20"-carbon steel. Note the undamaged areas of substrate (arrowed) revealed by spalling in (b).

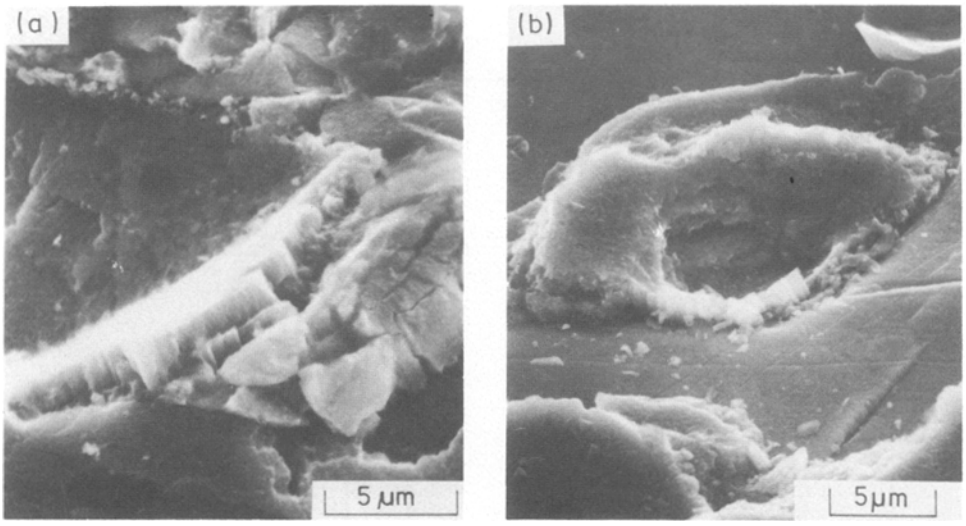

Figure 7 (a) Ploughed surface of 3.6 μm TiN on "20"-carbon steel after impact by alumina grit. Note the manner in which the coating has been pushed ahead of the impacting particle. (b) Impact site produced by alumina grit on 3 μm TiN on to stainless steel. Note that as in (a) the coating is pushed ahead of the particle. Also spallation of the coating surrounding the impact site is in evidence.

– plastic impact pits with no fracture or spallation are common (Fig. 8) – although some impact sites do show chipping (Fig. 8). It is apparent that extensive spalling has occurred for the 10 μm TiN on to stainless steel (Fig. 6b) as indicated by the large areas of revealed substrate that show no evidence of erosion (arrowed on Fig. 6b). Compared to both the thinner coatings (Figs 6a and c) and the 10 μm TiN/stainless steel coating, relatively little pitting and chipping is found on the thicker coatings on carbon steel (Fig. 6d). In addition, those regions of thick coating remaining on the stainless steel also showed good resistance to erosion (Fig. 6b). Clearly, the tendency for the coating to spall from the stainless steel substrate accounts for the poor resistance to erosion by angular particles when compared to the TiN coatings on "20"-carbon steel.

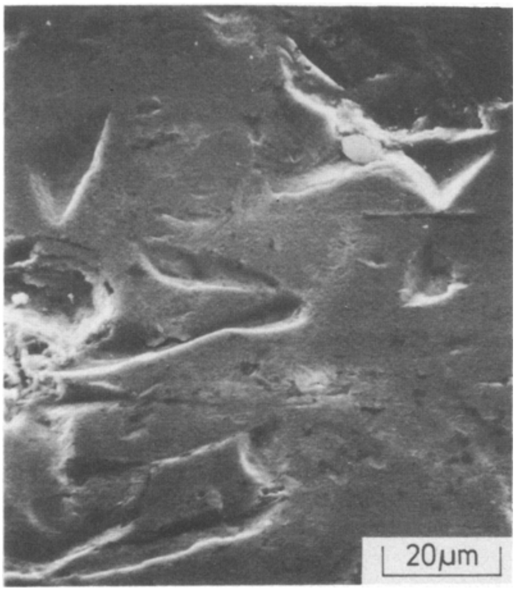

Figure 8 Scanning electron micrograph of the surface of 10.5 μm TiN on "20"-carbon steel after erosion by alumina grit at 14 m sec^{-1}. Note the plastic impressions caused by the impacting particles – some chipping fracture is also apparent.

In contrast to the erosion by angular particles, resistance to erosion by blunt particles is greater for the 3 μm coatings (see Fig. 5). SEM studies of the erosion surfaces (Fig. 9) reveal that, as for erosion by angular particles, the coatings on stainless steel have a tendency to spall (Figs 9a and b), the thicker coating appearing to spall after only a few impacts. Fig. 9b clearly shows individual impact sites (arrowed) in both the coating and exposed substrate on the 10 μm TiN/stainless steel specimen and, whilst there appears to be little damage associated with the impacts, large areas of coating have spalled. Similarly for the thin coating on stainless steel (Fig. 9a), areas of the coating have spalled close to impact sites, but to a lesser degree than for the thicker coating. Unlike the thick coating on to stainless steel where little impact damage within the adherent coating is seen (Fig. 9b), the thin coating shows cracking associated with impacts (Fig 10a). As with angular particle erosion the coating may deform and be pushed into the impact pits (Fig. 10b) or may spall under impact (Fig. 10c). The thin 3 μm TiN/carbon steel coating (Fig. 9c) shows considerably less impact damage than the thin 3 μm TiN/stainless steel coating of Fig. 9a. Again cracking associated with individual impacts is observed (Fig. 11a), and the interaction of these to form networks may give rise to pit formation (Fig. 11b). However, no spalling of the coating is observed indicating the level of practical adhesion is greater for the TiN/carbon steel system than the TiN/stainless steel system. The strength of this adhesion is apparent if the heavily bombarded surfaces are studied. Fig. 12a shows the appearance of a carbon steel surface from which the coating has been substantially eroded. However, using energy dispersive X-ray dot mapping (Fig. 12b) it is clear that a substantial amount of TiN remains adhered to, or embedded in, the surface. Figs 12c and d show such regions in greater detail and areas in which the columnar structure of the coating has been sheared by the impacting beads are apparent (arrowed).

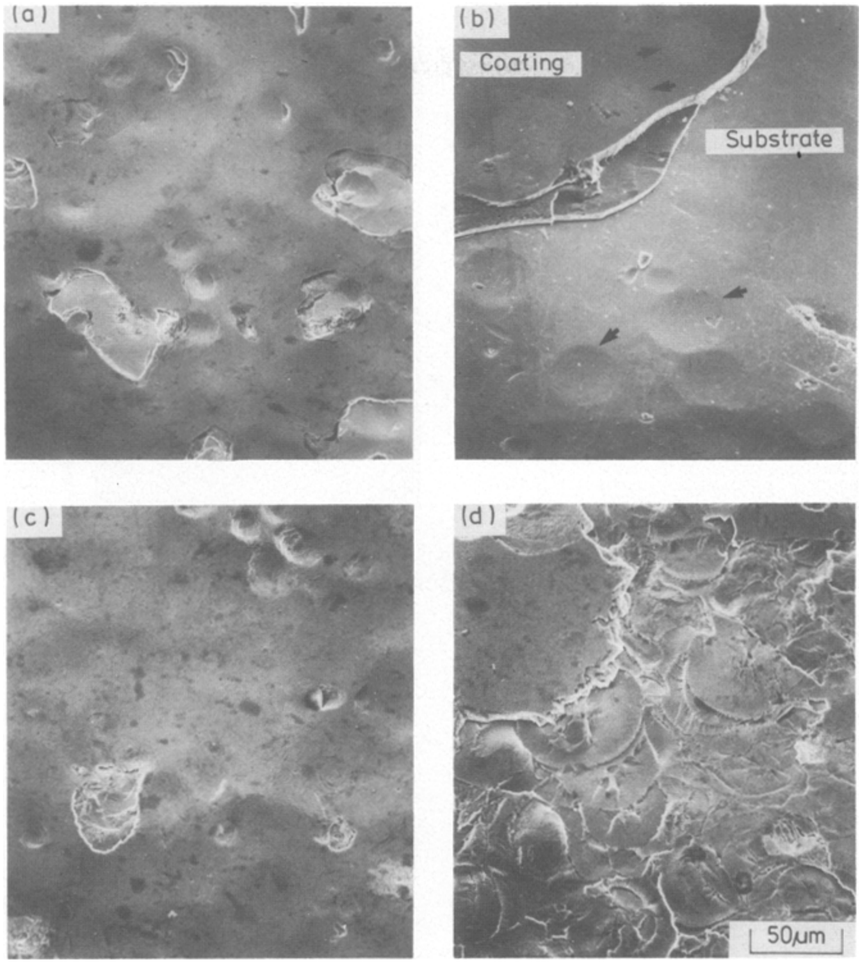

Figure 9 Scanning electron micrographs of TiN coated steels lightly eroded by glass beads at 24 m sec^{-1}. (a) 3 μm TiN on stainless steel, (b) 10 μm TiN on stainless steel, (3) 3.6 μm TiN on "20"-carbon steel and (d) 10.5 μm TiN on "20"-carbon steel. Note the individual impact sites (arrowed) on both coating and substrate in (b).

In contrast to the mechanisms of coating loss described above, erosion of the thick TiN/carbon steel coating shows a completely different surface morphology (see Figs 9d and 13). Each single impact has associated with it a saucer-like of "sombrero" shaped structure and nowhere was the substrate revealed by spalling. The origins of this "sombrero" fracture will be discussed in Section 4. Also, one other erosion pit

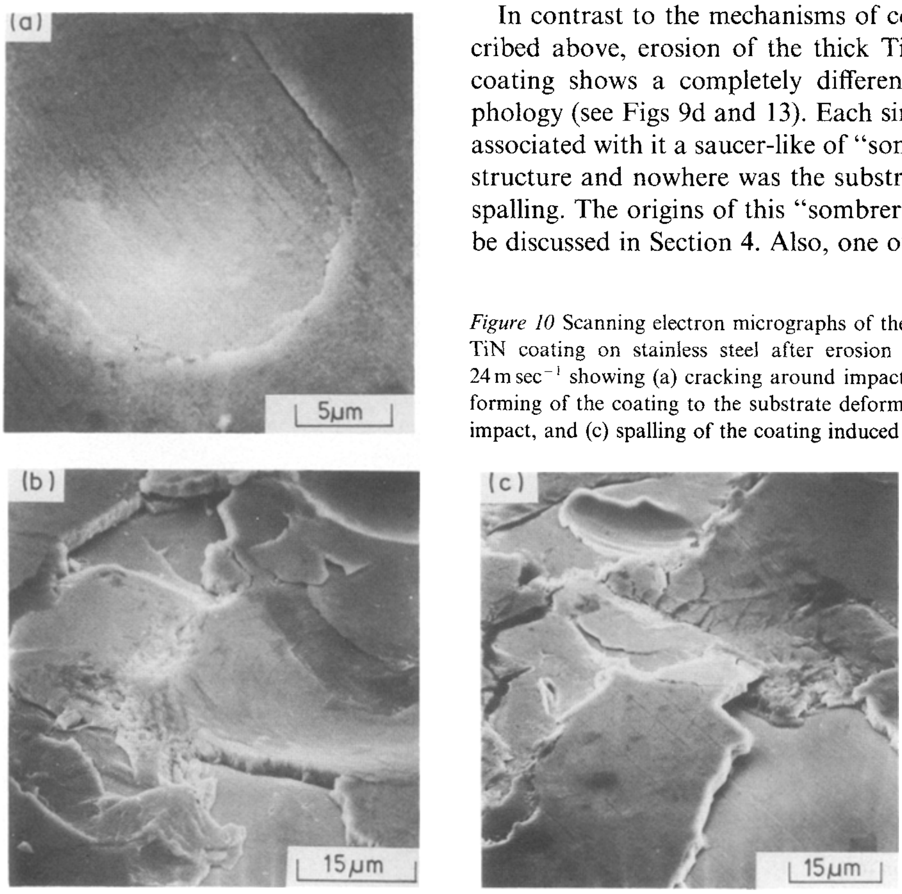

Figure 10 Scanning electron micrographs of the surface of a 3 μm TiN coating on stainless steel after erosion by glass beads at 24 m sec^{-1} showing (a) cracking around impact sites, (b) the conforming of the coating to the substrate deformation produced by impact, and (c) spalling of the coating induced by impact.

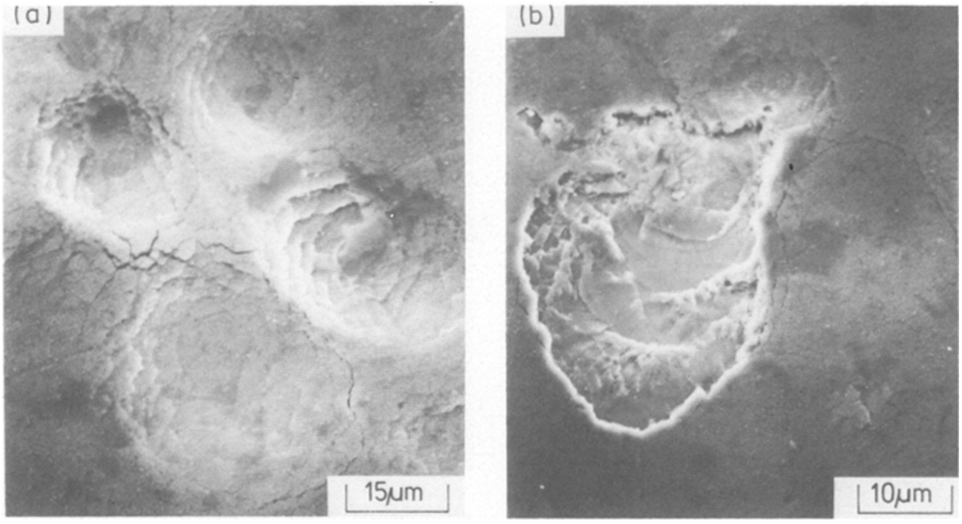

Figure 11 Scanning electron micrograph of impact sites from 3.6 μm TiN on "20"-carbon steel eroded by glass beads at 24 m sec^{-1}. (a) Showing the generation of crack networks by multiple impacts, and (b) an erosion pit generated by chipping of cracked coating such as that in (a).

structure was occasionally found on the TiN/stainless steel coatings which took the form of an inverted cone or crater at whose centre the substrate was revealed (Fig. 14).

3.3. Hardness

The hardness behaviour for the 3 and 10 μm coatings on both stainless steel and "20"-carbon steel were determined using the Burnett and Rickerby analysis [28, 29], and are given parametrically (as defined in Equation 1) in Table I. Within the limits of accuracy of the experimental hardness data the coating hardness (given at a 10 μm indentation size) lay between 2500 and 3000 VHN (24.5 to 29.4 GPa). These values are within the range of hardnesses found in the literature and expected from the present authors' work on

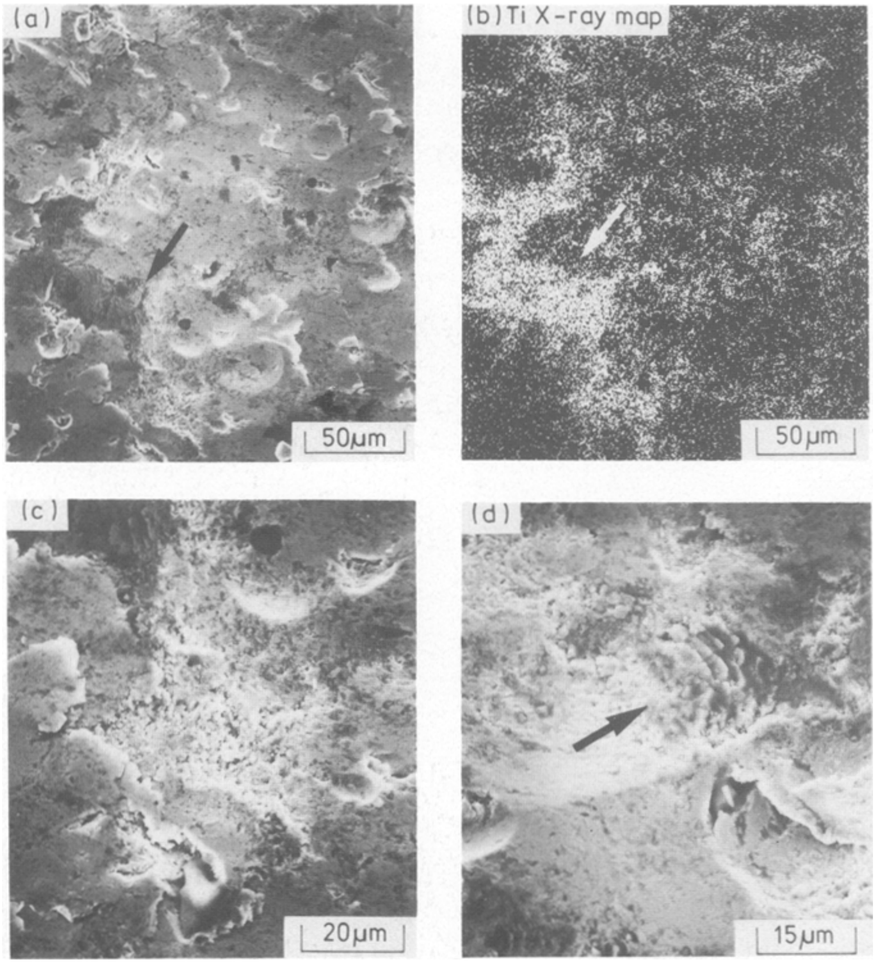

Figure 12 Surface morphology of TiN and "20"-carbon steel after heavy erosion by glass beads at 24 m sec^{-1}. (a), (b) 3.6 μm TiN after exposure to ~ 1200 g erodent showing regions of high titanium concentration associated with retained coating, (c) higher magnification of (a) showing heavily fractured coating, and (d) as (c) only for 10.5 μm TiN exposed to 500 g of erodent. Note the sheared columnar regions (arrowed) apparent in (d).

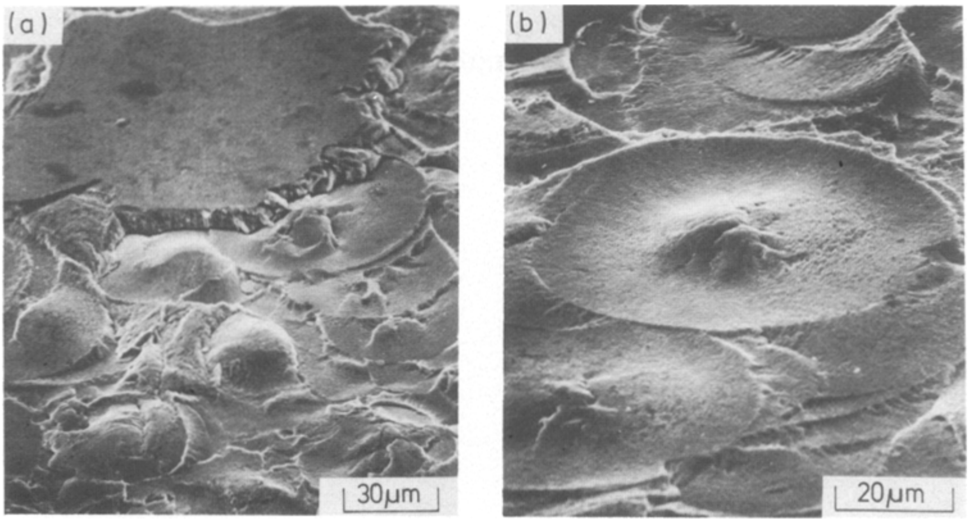

Figure 13 The appearance of 10.5 μm TiN lightly eroded by glass beads showing "sombrero" type fracture morphology. Note the presence of radial cracks in the "crown" of the sombrero featured in (b).

the variation of hardness of SIP titanium nitride with substrate bias during coating (see Section 2.1 and [24–26, 28, 29].

3.4. Scratch adhesion testing

The critical load (L_c) for coating failure was determined for all coatings by the inspection of the scratch track by light microscopy. Coatings were deemed to have failed when fracture occurred that revealed the substrate in a regular manner (with the exception of the thick TiN/carbon steel coating which failed cohesively). Several coating failure modes have been identified in the literature and are described in greater detail elsewhere [11–13, 19, 31]. The failure modes observed in the present study include: coating spallation ahead of and around the scratch track (Fig. 15); cohesive chipping of the coating, i.e. the substrate is not necessarily revealed (Fig. 16); regular chipping of the edges of the scratch to reveal substrate (Fig. 17a); formation of buckling failures ahead of the moving stylus (Fig. 17b); conformal cracking within the scratch with occasional coating loss from bottom of the track (Fig. 17c).

Both the L_c values and the principal coating failure mode for tests carried out on the erosion specimens are given in Table I. Inspection of Table I reveals several points worthy of note. Firstly, the value of L_c generally increases with thickness as shown in Table I and Fig. 18. Phenomenologically this has been attributed to the decay of the friction-induced interfacial shear stress as the coating/substrate interface is made increasing remote from the surface [11] and will be discussed in Section 4.2. Secondly, L_c for a given thickness is always less for TiN on stainless than TiN on "20"-carbon steel. Finally, the predominant failure mode is observed to change with increasing thickness, this also being reported by Je *et al.* [31]. The thinner coatings are generally seen to fail by loss of coating from the centre of the scratch associated with the formation of conformal crack networks whilst thicker coatings fail by spalling or cohesive cracking.

Fig. 18 is an attempt to correlate the scratch test results with the erosion behaviour and indicates the predominant failure modes in both scratch and erosion testing as a function of coating thickness. Clearly, spalling and cohesive coating loss occurs in thick coat-

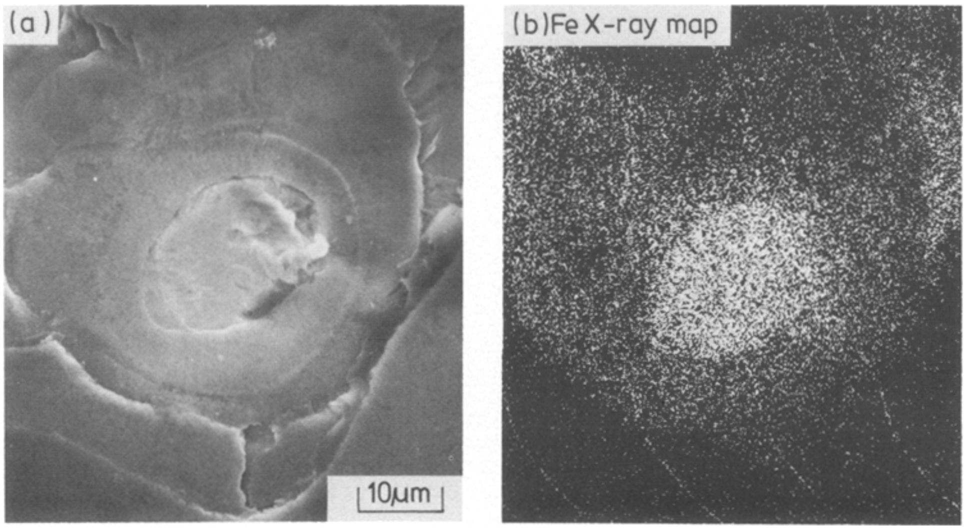

Figure 14 Scanning electron micrograph (a) and Fe X-ray dot map (b) of inverted cone fracture found on 3 μm TiN on stainless steel eroded by glass beads. In the central portion the substrate is exposed.

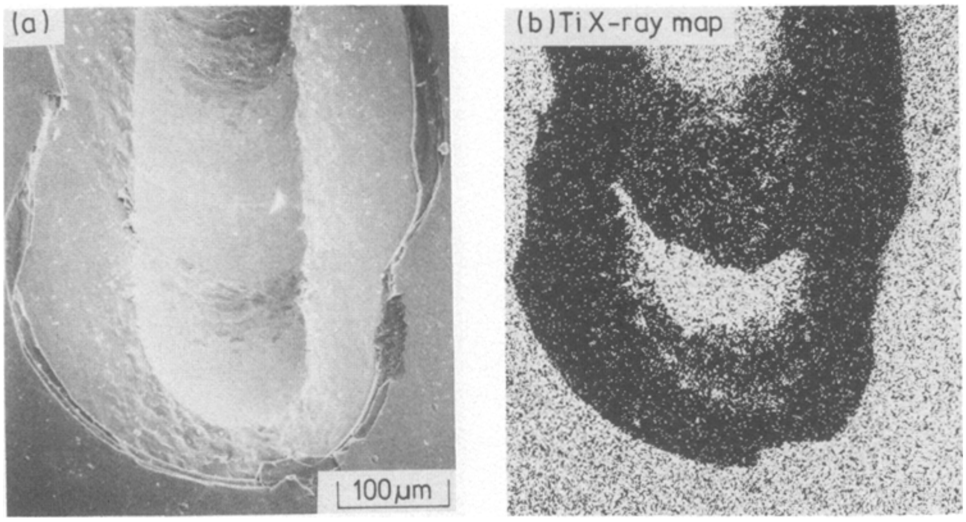

Figure 15 Scanning electron micrograph (a) and titanium X-ray dot map (b) of spalled coating from 10 µm TiN on stainless steel. The scratch load was 3800 g. Note the region of high titanium concentration in the track (b) corresponding to coating embedded in the substrate by passage of the stylus.

ings and these correlate with spalling and cohesive "sombrero" fracture under erosive conditions whilst conformal cracking and associated coating loss from the bottom of the scratch track can be seen to correlate with erosion by formation of crack networks (coupled with spalling for the stainless steel substrate). These correlations will now be discussed in greater detail.

4. Discussion

4.1. Erosion behaviour

For erosion by both angular particles and glass beads, the titanium nitride coatings on to stainless steel substrates were removed more rapidly than similar coatings deposited on to "20"-carbon steel. This behaviour may reflect poor interfacial adhesion (as distinct from practical adhesion) and/or decreased practical adhesion due to higher internal stresses. Laugier [32, 33] has suggested an energy balance approach to coating failure (specifically applied to the scratch test – see Section 4.2), whereby the energy required to create new surfaces by fracture along the coating–substrate interface has to be provided by the release of stored elastic energy. This approach predicts that highly stressed films (i.e. also possessing high levels of stored elastic energy) will fail under smaller mechanical loads than less internally stressed films. Clearly, the erosion behaviour of titanium nitride on to the two substrates in this study is consistent with such stress effects because the internal stress for the TiN/stainless steel systems is ~50% greater than for the TiN/"20"-carbon steel system. However, it is impossible to deduce anything concerning the strength of the interface itself.

Similarly the erosion behaviour of the TiN coated steels under impact by glass beads is of particular interest because for both substrates, the lifetime of the film decreases with increasing thickness. For the stainless steel substrate this can be rationalized by the use of the stored energy balance concept. This states that the total stored energy due to internal stress increases with film thickness (assuming the internal

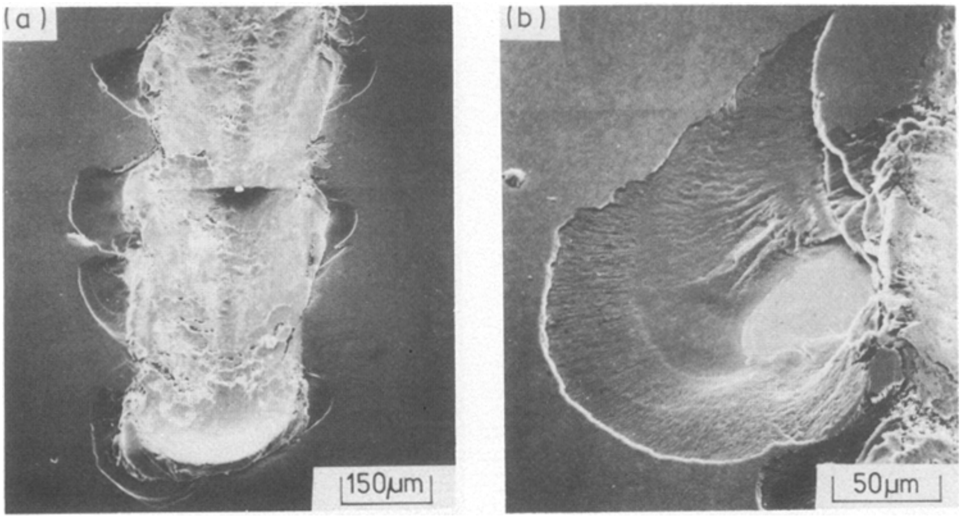

Figure 16 Scanning electron micrographs of cohesive chipping failure induced by the scratch test (load = 6400 g) on 10.5 µm of TiN on "20"-carbon steel. Note the extensive sloping fractures within the coating (e.g. in b) compared to the steep-sided fractures associated with spalling (Fig. 15a).

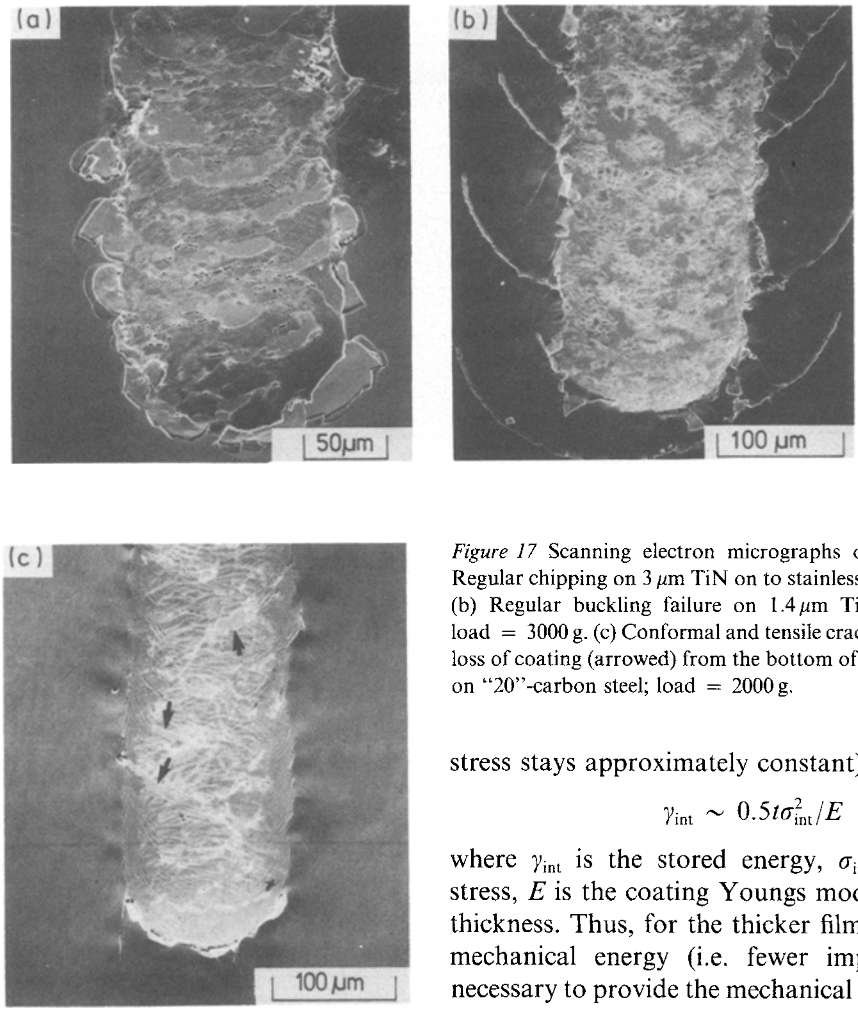

Figure 17 Scanning electron micrographs of scratch tracks. (a) Regular chipping on 3 μm TiN on to stainless steel; load = 2500 g. (b) Regular buckling failure on 1.4 μm TiN on stainless steel; load = 3000 g. (c) Conformal and tensile crack networks leading to loss of coating (arrowed) from the bottom of the track. 1.5 μm TiN on "20"-carbon steel; load = 2000 g.

stress stays approximately constant) according to

$$\gamma_{\text{int}} \sim 0.5t\sigma_{\text{int}}^2/E \qquad (2)$$

where γ_{int} is the stored energy, σ_{int} is the internal stress, E is the coating Youngs modulus and t is the thickness. Thus, for the thicker films, less additional mechanical energy (i.e. fewer impacts) would be necessary to provide the mechanical stimulus for coating detachment; in agreement with the experimental

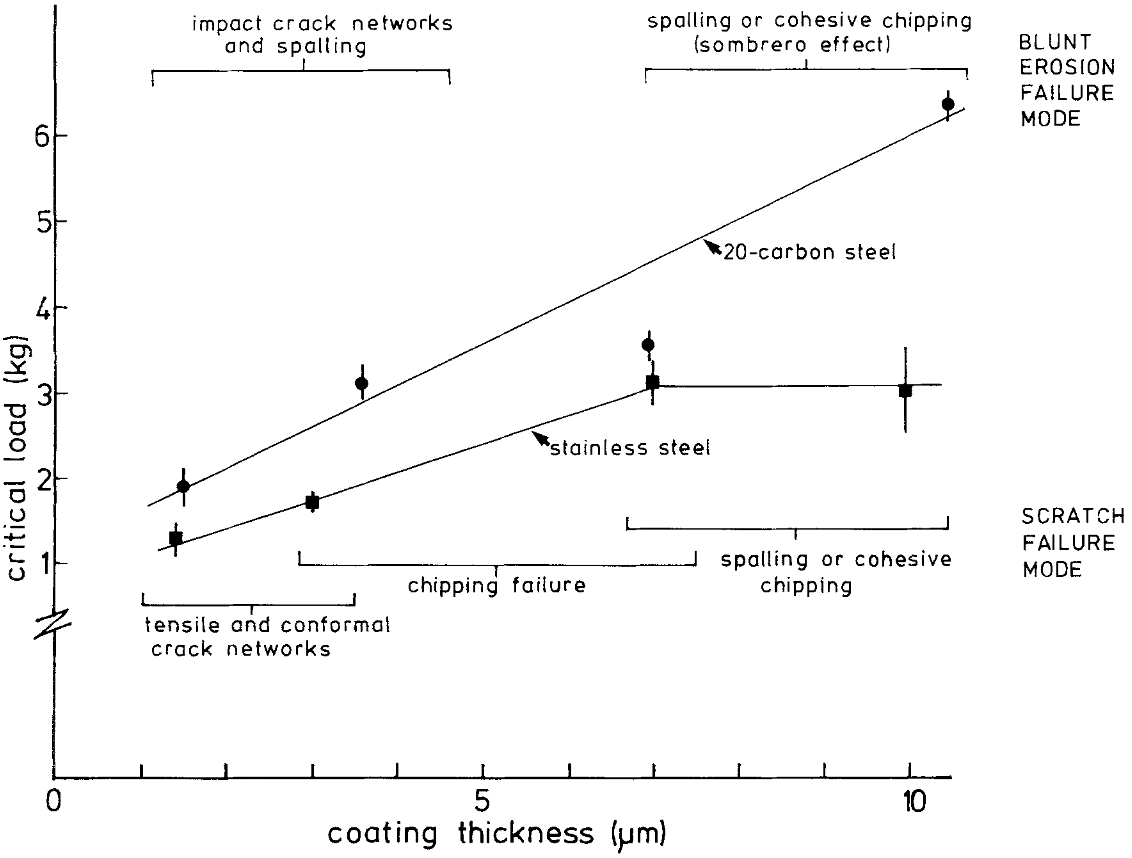

Figure 18 The variation of critical load for coating loss, L_c, with coating thickness for TiN on stainless steel and "20"-carbon steel substrates. Also indicated are the scratch and erosion failure modes observed.

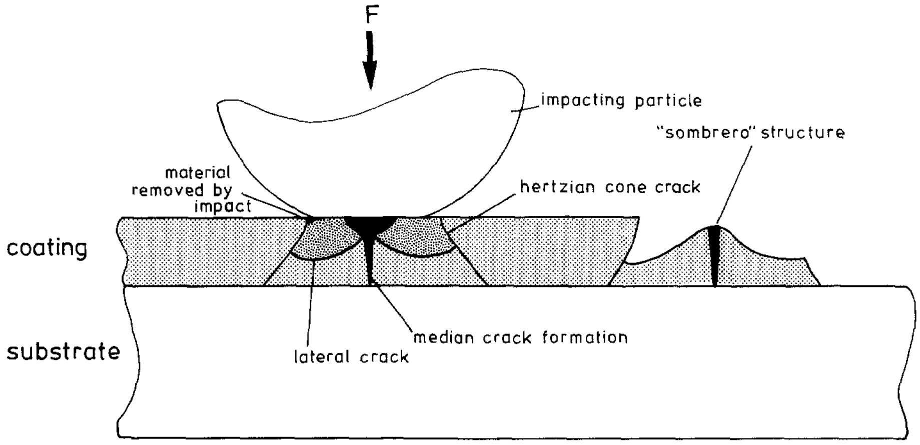

Figure 19 A schematic representation of the mechanism by which the "sombrero" structures of Fig. 13 are formed by the intersection of cone cracks with lateral cracks.

results presented in Figs 5 and 9. In thicker coatings, the spallation of large areas with little apparent damage to the substrate indicates that a shock wave loading mechanism may be responsible for the initiation of spallation failures. In contrast, the 10 μm TiN coating on "20"-carbon steels fails by cohesive failure.

During the early stages of erosion of thick titanium nitride coatings deposited on to carbon steel, each impact gives rise to a "sombrero" structure as shown in Fig. 13. This contrasts with the Hertzian cone fractures [34], reported during erosion of brittle materials by blunt erodents where the diameter of the crack at the surface, *d*, is approximately the elastic contact diameter; these cones being similar to those formed by blunt (elastic) indentation of brittle materials [35]. However, erosion of brittle materials by angular particles produces a chipping fracture mechanism akin to the lateral crack formation associated with sharp contacts [36]. Consequently, the "sombrero" morphology may arise from the simultaneous formation of both Hertzian cone fractures and the median/radial/lateral indentation fracture morphology commonly found in ceramics [37]. Therefore, under dynamic impact conditions there is a transition between the two fracture forms, the blunt particles appearing increasingly "sharp" as the impact velocity increases; the co-existence of cone and median/radial/lateral crack systems has been reported in the literature [36]. Clearly from Fig. 13 it can be seen that the radius of the "brim" of the sombrero ($\sim 50\,\mu$m) is approximately the same as the contact diameter as can be seen in Fig. 9 for instance. This supports the premise that the maximum extent of the sombrero is determined by the Hertzian cone profile. Fig. 19 shows schematically the formation of these sombrero structures, the wide curving brim being formed by the propagation of lateral cracks out from the centre of the impact until they intersect the cone crack that has simultaneously propagated downwards. The radial cracks play no part in this process but may be seen clearly in the crown of the sombrero (Fig. 13b).

Whilst it is clear that rapid coating loss will occur as a consequence of spalling, driven by elastic energy release and initiated by impact-induced shock wave loading, it is less clear why cohesive failure of a thick coating also results in more rapid removal of the coating. Although impact of the TiN/carbon steel coating results in the formation of "sombrero" fractures, the substrate still remains fully covered by coating in the early stages of erosion – coating loss not being as catastrophic as for TiN/stainless steel systems. However, the remaining layer of coating is clearly removed more rapidly than a new, unbombarded coating of equivalent thickness. This can be attributed to the remaining layer of coating being highly fractured, because both the Hertzian cone cracks and radial cracks formed on impact will extend down to the coating/substrate interface; only a little extra impact is required to remove this residual material. However, no Hertzian cone or ring cracks are seen on the bead-bombarded thin coatings (Figs 10 and 11). This indicates that there may be a critical coating thickness beneath which cone and/or median/radial/lateral fracture does not occur. But studies of the erosion behaviour of TiN-coated glass do show that Hertzian ring cracking can occur on coatings as thin as 0.5 μm [36]; this indicates that the nature of the substrate might be important. For the thin TiN coatings, impact by the glass beads used here results in plastic deformation of both substrate and coating (Figs 10 and 11), the coating conforming to the profile of the impact pit whilst remaining adherent. Hertzian fracture, and to a lesser extent median/radial/lateral fracture, are elastic contact phenomena. Clearly, as the coating is thickened, the hardness and stiffness of the surface "experienced" by the impacting spheres increases until the surface appears sufficiently hard and stiff to allow the generation and support of stresses sufficient to initiate fracture, i.e. the coated surface behaves more like a bulk ceramic. Clearly, the cone-cracks are a crucial feature of the coating removal process. Their absence during angular particle erosion explains why thicker coatings show greater erosion resistance, whilst under blunt erosion their occurrence enhances coating loss.

It is interesting to compare this behaviour to that reported for columnar NiO scales eroded by angular particles [9]. In this work a two-stage erosion mechanism was observed. Initially the outer layer of the oxide was removed by median/radial/lateral chipping. Polishing away the surface layers of the oxide in order to study the sub-surface fracture in the scale revealed Hertzian fracture extending to the oxide/metal interface. In this work the "sharp" particles had appeared "blunted" by a cap of plastically deforming material beneath the impact site, this then can act as a blunt indentor to produce Hertzian cone fracture. Clearly, this co-existence of Hertzian and median/radial/lateral fracture forms parallel the results here to a limited extent and indicates that often fracture morphologies do not fall into a simple category.

The erosion behaviour of the titanium nitride coatings eroded by angular particles is similar for both substrates – plasticity induced chipping akin to the elastic/plastic indentation fracture morphology found in ceramics [35–37] being the predominant mechanism for coating removal. However, a certain amount of spalling accompanies the chipping on both TiN/stainless steel specimens. Both of the thicker coatings appear to deform less under impact, often only a plastic impression being formed at the impact sites. In contrast, the impact of the thinner coated surfaces results in plastic deformation of the substrate, the coatings being pushed into the substrate – clearly as the coatings thicken the effective surface hardness increases with the consequence that the impact damage is significantly contained with the coating. The increased erosion resistance of the thicker coatings is probably a consequence of this localization of impact damage. The coating is no longer grossly deformed as observed for the thin coatings and consequently stays intact for longer.

Finally, the inverted cone fracture morphology shown in Fig. 14 may be a result of shock wave loading at the interface. Impact and laser pulse techniques have both been used to generate shock waves within the coating that, when reflected at the coating/substrate interface, result in strong tensile stresses being formed at that interface which cause coating delamination. The morphology of the pit indicates that the coating was "hit from behind", this being consistent with a shock wave induced failure.

4.2. Scratch behaviour

As was noted in Section 3.4, the critical load for coating failure was observed to increase with thickness and that, for a given thickness, the L_c values for TiN coatings on stainless steel were consistently lower than similar coatings on "20"-carbon steel. The role of substrate deformation, and the way in which load support is partitioned upon L_c have been discussed in the literature (e.g. [11]), a result commonly found being that L_c increases with substrate hardness. However, in the present study the "20"-carbon steel had a hardness of ~ 130 VHN (1.3 GPa) compared to the stainless steel which had a hardness of ~ 180 VHN (1.8 GPa). Clearly, solely on the load support argument discussed elsewhere [11] the L_c values should be greater for the TiN coatings on stainless steel substrates. In addition, using the plastic zone mismatch analysis developed and described by Burnett and Rickerby [13, 19], the interfacial shear stress due to the indentation stress field will be ~ 20% greater for TiN on the softer "20"-carbon steel – again, all other things being equal, this would result in a lower L_c for the carbon steel substrate. Using both the energy balance approach and the critical interface shear stress criteria for coating loss, the presence of a high internal stress is expected to result in a lower L_c as observed. In the present study, the internal stresses are several times higher than the stresses generated by the indentation plastic zone mismatch (maximum value of ~ 2 GPa at the coating elastic/plastic boundary) and much higher than any differences in plastic zone mismatch stress between the two substrates (estimated as ~ 0.4 GPa compared to 2 GPa difference in internal stress between carbon steel and stainless steel substrates) and so the internal stress level dominates coating failure. The effects of stress on L_c have been highlighted by the present authors in a series of experiments where the substrate remained constant but the internal stress level was varied by controlling the substrate bias during coating. Again, L_c was observed to decrease with increasing stress. As before, it is impossible to determine anything about the relative strengths of the TiN/stainless steel and TiN/carbon steel interfaces themselves. Undoubtedly, the internal stress states present in the TiN coatings do contribute to the differences in L_c, but there may (or may not) also be significant differences in the actual interfacial adhesion strengths.

The coating failure mode was observed to vary with thickness (t). When $t \leqslant 3\,\mu$m, coating failure was generally by loss of material from within the track, this arising due to the creation of crack networks as the coating conforms to the plastic deformation induced by the stylus (Fig. 17c). In addition, the action of the frictional forces between coating and stylus causes the columnar units to be pulled over (Fig. 20) and in some cases the combination of the frictional traction and crack networks results in coating being "plucked" from the bottom of the track.

At greater thicknesses (3 to 8 μm) this mode of failure becomes augmented by chipping, principally at the edges of the track. Finally, for well-adhered thick coatings (> 10 μm) the coating starts to behave as a bulk ceramic, cohesive chipping occurring along the track. For the weakly bonded coatings spallation becomes the predominant failure mechanism. The driving force of the former failure mode in the elastic/plastic indentation stress field that gives rise to the median/radial/lateral crack system during static indentation of ceramics (e.g. [34]). In the latter case, spallation failure appears to be driven by the release of elastic energy by propagation of fracture along the interface. The elastic energy released will consist of two components, an indentation stress field component and the internal stress. Marshall *et al.* [17, 18] have modelled the fracture mechanisms for this mode of failure around static indentation. It is important to realize that whilst L_c increases with thickness, the fracture mode changes and hence the information conveyed by L_c also changes. Thus, at best L_c is only a measure of the response of a system to a specific mechanical loading situation, and whilst it does depend upon interfacial adhesion, it is equally dependent upon a large number of "extrinsic" parameters such as substrate, thickness, etc. However, despite these reservations, the morphology of the coating loss, as revealed by the scratch test, does allow correlations

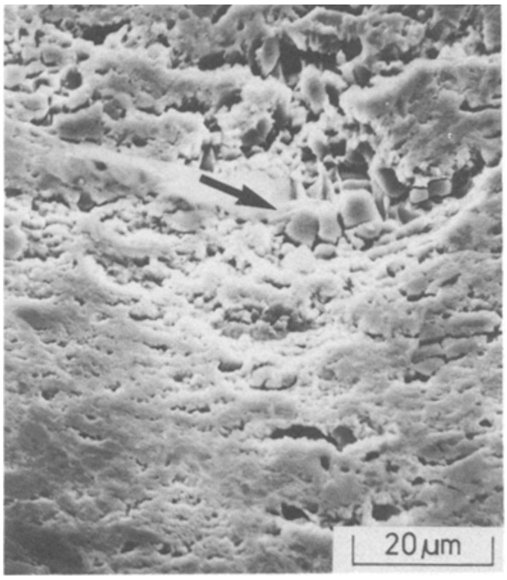

Figure 20 Sheared blocks of coating in the bottom of a scratch track (arrowed).

with erosion behaviour to be made and will now be discussed in greater detail.

4.3. Correlation between erosion and scratch behaviour

4.3.1. *Angular particle erosion*

The mode of coating loss under erosion by the alumina grits correlates with the scratch failure mode; for instance, the predominant coating failure mechanism for the coated "20"-carbon steel substrate is by elastic/plastic chipping in both the scratch and erosion tests. In contrast, the TiN coating on the stainless steel substrate showed a tendency to spall under both erosion and scratch testing. It is also interesting to note that mass of erodent for coating loss under erosion increases with coating thickness, and this can be correlated with L_c. For the TiN/stainless steel system, the mass of erodent for coating loss only increases slightly with thickness, whereas for the TiN/"20"-carbon steel a larger increase is found; this correlates with increases in L_c from 1700 to 3100 g and from 3100 to 6300 g, respectively.

4.3.2. *Blunt particle erosion*

Clearly, unlike erosion by angular particles, L_c cannot be sensibly correlated with erosion resistance because thicker coatings erode faster but have higher L_c values. However, a correlation does exist between the erosive loss mechanism and the scratch failure mode (see Fig. 18). On both carbon steel and stainless steel substrates the thinner coatings fail by (principally) the formation of crack networks by multiple impact, these regions of weakened material may then be eroded to form pits which then grow to reveal the substrate. For the stainless steel substrate this process is enhanced by a limited amount of spalling. This correlates well with the scratch behaviour of the 3 µm coatings. For the thicker coatings, the failure mechanisms correlate well with those observed in the scratch test, cohesive chipping occurring in the TiN/"20"-carbon steel coating and spalling in the TiN/stainless steel coatings.

5. Conclusions

The results presented in the previous section allow some broad conclusions to be drawn concerning the erosion behaviour of sputter-ion-plated TiN coatings on steels.

It has been shown that thicker coatings provide greater erosion resistance than thinner coatings when subjected to impact by angular erodent particles. Conversely, it has been found that the thicker coatings are lost more readily under erosion by blunt particles and has been attributed to the formation of Hertzian cone fractures and elastic/plastic "indentation" fractures once a critical coating thickness has been exceeded.

Sputter-ion-plated titanium nitride coatings deposited on to stainless steel erode faster than similar coatings deposited on to "20"-carbon steel and this has been correlated with an increased tendency for the TiN to spall from the stainless steel under impact. This spallation is believed to be driven by the high levels of elastic strain energy present in the coating as a result of the presence of high internal (residual) stresses.

Scratch adhesion testing may be correlated with erosion behaviour in several ways. Spallation failure induced by the scratch test has been found to indicate the probable occurrence of spallation during erosion. Similarly, cohesive failure induced by the scratch test may be reflected by cohesive failure under erosive conditions. However, the critical load for coating failure, L_c, is an unreliable guide to coating performance under erosion because increases in L_c with thickness correlate with increases in erosion resistance only for erosion by angular particles, the reverse being true for erosion by blunt particles.

Thus, this paper has described the scratch and erosion behaviour of a variety of TiN-coated samples and identified the mechanisms for coating loss. It has been shown that studies of the coating failure modes induced by the scratch test can be correlated with erosive loss mechanisms; however, no correlation can be made to enable prediction of relative erosion rates from the results of the scratch test.

Acknowledgements

The authors thank the Department of Trade and Industry for financial support. Mr T. J. Betts is thanked for performing microhardness and scratch tests and Mr B. A. Bellamy and Mr A. Jones are thanked for the X-ray work. This paper is published by permission of UKAEA, holders of the copyright.

References

1. A. BENNETT, *Mater. Sci. Technol.* **2** (1986) 257.
2. H. E. HINTERMANN, *J. Vac. Sci. Technol. B* **2** (1984) 816.
3. D. G. BHAT and P. F. WOERNER, *J. Metals* **38** (February) (1986) 68.
4. E. NIEMI, A. S. KORHONEN, E. HARJU and V. KAUPPINEN, *J. Vac. Sci. Technol. A* **4** (1986) 2763.
5. A. LEVY, D. BOONE, A. DAVIS and E. SCHOLZ, Proceedings 6th International Conference on Erosion by Liquid and Solid Impact, edited by J. E. Field and N. S. Corney (Cavendish Laboratory, Cambridge, 1983) pp. 46-1.
6. B. JONSSON, L. AKRE, S. JOHANSSON and S. HOGMARK, *Thin Solid Films* **137** (1986) 65.
7. D. S. RICKERBY, *J. Vac. Sci. Technol. A* **4** (1986) 2809.

8. L. CHOLLET and A. J. PERRY, *Thin Solid Films* **123** (1985) 223.
9. G. ZAMBELLI and A. V. LEVY, *Wear* **68** (1981) 305.
10. S. HOGMARK, A. HAMMARSTEN and S. SODERBERG, Proceedings 6th International Conference on Erosion by Liquid and Solid Impact, edited by J. Field and N. S. Corney (Cavendish Laboratory, Cambridge, 1983) pp. 37-1.
11. A. J. PERRY, *Surface Engng* **2** (1986) 183.
12. J. VALLI, *J. Vac. Sci. Technol. A* **4** (1986) 3007.
13. P. J. BURNETT and D. S. RICKERBY, *Thin Solid Films* **157** (1988) 233.
14. W. E. SNOWDEN and I. A. AKSAY, in "Surfaces and Interfaces in Ceramic and Ceramic-Metal Systems", edited by J. Pask and A. Evans (Plenum, New York, 1981) p. 651.
15. J. L. VOSSEN, in "Adhesion Measurement of Thin Films, Thick Films and Bulk Coatings", edited by K. L. Mittal, Special Tech. Pub. 640, (ASTM, Philadelphia, 1978) p. 122.
16. S. S. CHIANG, D. B. MARSHALL and A. G. EVANS, in "Surfaces and Interfaces in Ceramic and Ceramic-Metal Systems", edited by J. Pask and A. Evans (Plenum, New York, 1981) p. 603.
17. D. B. MARSHALL and A. G. EVANS, *J. Appl. Phys.* **56** (1984) 2632.
18. C. ROSSINGTON, D. B. MARSHALL, A. G. EVANS and B. T. KHURI-YAKUB, *ibid.* **56** (1984) 2639.
19. P. J. BURNETT and D. S. RICKERBY, *Thin Solid Films* **154** (1987) 403.
20. R. A. DUGDALE, Proceedings International Conference on Ion Plating and Applied Techniques (CEP Consultants, Edinburgh, 1977) p. 177.
21. J. P. COAD and R. A. DUGDALE, Proceedings International Conference on Ion Plating and Allied Techniques (CEP Consultants, Edinburgh, 1979) p. 186.
22. U. HELMERSSON, B. O. JOHANSSON, J.-E. SUNDGREN, H. T. G. HENTZELL and P. BILLGREN, *J. Vac. Sci. Technol. A* **3** (1985) 308.
23. D. S. RICKERBY and P. J. BURNETT, (1987) in preparation.
24. D. S. RICKERBY and P. J. BURNETT, *Thin Solid Films* **157** (1988) 195.
25. *Idem*, AERE Report No. R-12360, October (1986).
26. J.-E. SUNDGREN, *Thin Solid Films* **128** (1985) 21.
27. A. W. RUFF and L. K. IVES, *Wear* **35** (1975) 195.
28. P. J. BURNETT and D. S. RICKERBY, *Thin Solid Films* **148** (1987) 41.
29. *Idem, ibid.* **148** (1987) 51.
30. P. M. SARGENT and T. F. PAGE, *Proc. Brit. Ceram. Soc.* **26** (1978) 209.
31. J. H. JE, E. GYARMATI and A. NADOUMIDIS, *Thin Solid Films* **136** (1986) 57.
32. M. T. LAUGIER, *ibid.* **117** (1984) 243.
33. *Idem, J. Mater. Sci.* **21** (1986) 2269.
34. W. F. ADLER, *Wear* **37** (1976) 345.
35. B. R. LAWN and T. R. WILSHAW, *J. Mater. Sci.* **10** (1975) 1049.
36. A. W. RUFF and S. M. WIEDERHORN, *Treatise Mater. Sci. Technol.* **16** (1979) 69.
37. B. R. LAWN and D. B. MARSHALL, *J. Amer. Ceram. Soc.* **62** (1979) 347.
38. P. J. BURNETT and D. S. RICKERBY, Proceedings 7th International Conference on Erosion by Liquid and Solid Impact, edited by J. E. Field, Cambridge 1987, (Cavendish Laboratory, Cambridge) in press.

*Received 17 June
and accepted 27 August 1987*